

Near-field Beamforming for Extremely Large-scale MIMO Based on Unsupervised Deep Learning

Jiali Nie, Yuanhao Cui, *Member, IEEE*, Zhaohui Yang, *Member, IEEE*, Weijie Yuan, *Member, IEEE*, Xiaojun Jing *Member, IEEE*

Abstract—Extremely Large-scale Array (ELAA) is considered a frontier technology for future communication systems, pivotal in improving wireless systems' rate and spectral efficiency. However, as ELAA employs a multitude of antennas operating at higher frequencies, users are typically situated in the near-field region where the spherical wavefront propagates. This inevitably leads to a significant increase in the overhead of beam training, requiring complex two-dimensional beam searching in both the angle domain and the distance domain. To address this problem, we propose a near-field beamforming method based on unsupervised deep learning. Our convolutional neural network efficiently extracts complex channel state information features by strategically selecting padding and kernel size. We optimize the beamformers to maximize achievable rates in a multi-user network without relying on predefined custom codebooks. Upon deployment, the model requires solely the input of pre-estimated channel state information to derive the optimal beamforming vector. Simulation results show that our proposed scheme can obtain stable beamforming gain compared with the baseline scheme. Furthermore, owing to the inherent traits of deep learning methodologies, this approach substantially diminishes the beam training costs in near-field regions.

Index Terms—Extremely Large-scale Array (ELAA), near-field, beamforming, deep learning.

I. INTRODUCTION

THE sixth-generation (6G) wireless communication networks demand heightened spectral efficiency, reduced power consumption, as well as increased antenna numbers and densities to facilitate faster and more reliable data transmission, catering to the evolving needs of future intelligent systems, Internet of Things, and other fields [1], [2], [3]. Under this vision, the extremely large-scale antenna array (ELAA) is considered one of the important ways to achieve the 6G key performance indicators [4]. As wireless communications transition towards high frequency in millimeter wave (mmWave) and terahertz (THz) bands, ELAA is expected to be widely deployed on the base station (BS), aiming to offset the pronounced path losses stemming from highly focused beamforming. [5], [6], [7].

Manuscript received xx; revised xx; accepted xx. Date of publication xx. (Corresponding author: Yuanhao Cui.)

Jiali Nie and Xiaojun Jing are with the School of Information and Communication Engineering, Beijing University of Posts and Telecommunications, Beijing 100876, China (e-mail: niejl@bupt.edu.cn; jxiaojun@bupt.edu.cn).

Yuanhao Cui and Weijie Yuan is with the Department of Electrical and Electronic Engineering, Southern University of Science and Technology, Shenzhen 518055, China (e-mail: cuiyh@sustech.edu.cn; yuanwj@sustech.edu.cn).

Zhaohui Yang is with the College of Information Science and Electronic Engineering, Zhejiang University, Hangzhou, Zhejiang 310027, China (e-mail: yang_zhaohui@zju.edu.cn).

However, as the carrier frequency and the number of antennas increase, the Rayleigh distance in the communication systems gradually expands, reaching tens to hundreds of meters [8]. For instance, in the case of an ELAA with a 1 meter aperture operating at 60 GHz, the Rayleigh distance can extend up to 400 meters. The interactions among antennas become dense and intricate, leading to the so-called near-field signal propagation properties. The area within the Rayleigh distance is known as the near field, whereas the region beyond this distance is referred to as the far field [9]. This near-field effect primarily manifests in the signal propagation mode transitioning from plane wave propagation to spherical wave propagation [10].

Near-field communications present distinct advantages in enhancing communication coverage and signal quality, especially for high-density signal coverage scenarios such as indoor environments or dense urban areas. Leveraging the unique propagation characteristics of the near field enables flexible beam focusing, allowing for precise localization of beam energy onto specific spatial positions rather than a specific angle as in traditional far-field communications paradigms [11].

While near-field communications boasts advantages, it encounters substantial challenges in channel modeling, channel estimation, and beamforming due to the inapplicability of schemes designed for far-field scenarios. Specifically, in near-field communications, the beam codebook must account for both angle and distance sampling [12]. Compared with far-field codebooks involving angles sampling only, the beam codebook of near-field necessitate encompassing more candidate beams, thereby rendering the cost of beam training prohibitive. Hence, the near-field beam training of ELAA remains a formidable research endeavor.

A. Related works

1) *Near-field Communications*: Near-field communications utilize ELAA to improve the performance of wireless systems. A larger antenna size and array aperture of ELAA will bring a higher beamforming gain, but it will also lead to increased precoding complexity, more challenging beam management, and growing power consumption [13], [14], [15]. Currently, numerous researchers have carried out research on ELAA near-field communications. Existing massive multiple-input multiple-output (MIMO) systems typically operate under narrowband assumptions, with beamforming and antenna spacing tailored to center frequencies [16]. However, the traditional

beamforming architecture in near-field wideband systems may cause beam deflection and potentially even beam splitting [17]. Furthermore, concerning codebook design, the near-field channel no longer has the sparsity in the angle domain, which makes the far-field-based orthogonal angle domain Discrete Fourier transform (DFT) codebook no longer applicable [18]. The spherical propagation of near-field signals makes the distance of the antenna to user equipment (UE) different. The near-field array response vector is determined not only by the direction of the BS and the UE but also by the distance. This will greatly increase the complexity of near-field codebook design [19].

Changes in the electromagnetic propagation of the near-field region also bring new opportunities for 6G wireless communications. Unlike far-field communications, near-field communications can leverage enhanced range resolution to serve multiple UEs simultaneously [20]. This feature provides additional degrees of freedom (DoF) to enhance system capacity and reduce inter-user interference [21], [22]. Near-field communications also have great potential applications in perception and security. The authors of [23] proposed a near-field integrated sensing and communications (ISAC) framework, which provides additional distance dimensions for both sensing and communications. The inclusion of an extra distance dimension in near-field ISAC leads to performance improvements compared to far-field ISAC. Moreover, [24] proposed the concept of near-field non-orthogonal multiple access (NF-NOMA) to enable continuous interference elimination from far to nearby focusing beamformers at specific locations. Near-field communications' ability to discern distance differences between UEs can significantly enhance physical layer security and communication confidentiality [25].

2) *Traditional Far-field Beamforming*: Traditional beam training typically involves pilot training and beam alignment. In the pilot training phase, the transmitter sends a series of pilot signals covering different beam directions, and the received signals are adopted to estimate channel state information (CSI) [26]. During the beam alignment phase, the receiver feedbacks estimated information to the transmitter, prompting adjustments to the beamformers to optimize signal focus on the receiver. Many works have been done on far-field beam training and codebook design to improve beam training accuracy and reduce overhead. Specifically, to address the high power consumption associated with fully digital beamforming, [27] developed a heuristic hybrid beamforming scheme that achieves performance levels close to those of full digital beamforming. An efficient hierarchical codebook was developed using sub-array and deactivated antenna technology in [28]. It utilizes the results of beam training from the previous layer as the code words for the current layer, resulting in a substantial reduction in beam training overhead. An enhanced layered codebook beam training scheme is proposed in [29] to minimize propagation errors between adjacent beams. Based on the beam pattern, the power threshold of the received signal and the misalignment probability of the beam are analyzed to improve the accuracy of the beam alignment significantly.

However, the far-field beamforming method presents challenges when dealing with near-field beams because the near-

field UE channel is not only affected by the angle of departure/angle of arrival (AoD / AoA) but also by the spatial distance. Using far-field beamforming techniques for near-field training can lead to an energy diffusion effect, i.e., the beam energy directed at a specific angle may disperse to multiple angles. This direct application of far-field beam training methods to near-field scenarios may cause significant performance degradation.

3) *Near-field Beamforming*: To address the above issue, extensive research has been conducted on near-field beamforming techniques. Specifically, [30] proposed a near-field codebook that simultaneously extracts angle and distance information. This approach reduces the codebook size to a certain extent by designing a polar transformation matrix for uniform sampling in the angle domain and non-uniform sampling in the distance domain. For near-field communications, a two-stage layered beam training method was introduced in [31]. In the initial stage, the traditional far-field codebook is employed to conduct a rough search for candidate UE's directions in the angle domain. Subsequently, in the second stage, a specially designed polar codebook is utilized to refine the search for UE's distances within the candidate angle. Beam splitting induced by wideband ELAA was ingeniously utilized in [32] for beam search, achieving efficient near-field beam training with minimal overhead. The proposed method employs time delay (TD) beamforming to regulate the near-field beam splitting, enabling the search for the optimal angle through frequency division and the optimal distance ring through time division. Furthermore, a near-field beam training scheme leveraging deep learning was introduced in [33]. This approach utilizes a specialized codebook containing angle and distance information to train a deep learning model, empowering it to autonomously predict the optimal angle and distance.

Nonetheless, the escalation of antenna size and codebook complexity exacerbates the overhead of beam training in near-field communications, as previously mentioned. Therefore, it is imperative to devise a low-overhead algorithm to mitigate the challenges posed by ELAA communication systems.

B. Key idea

Deep learning technology is widely used in wireless communication scheme design due to its powerful feature extraction and learning capabilities. By conducting offline training and online deployment of deep learning models for near-field beam training, computational overhead can be substantially minimized, thus aligning with the requirements of practical applications. In this subsection, we delve into three specific considerations when designing deep neural networks in near-field beamforming.

Beamforming vector modulus constraints: Regarding the amplitude constraints of beamforming vectors our innovative application of Euler's formula presents an elegant solution. The output layer function is structured to guide the neural network in outputting the direction of the beamforming vector, rather than its numerical value directly. Subsequently, Euler's formula is incorporated into the loss function to convert angles

into numerical values, ensuring adherence to the specified modulus of the beamforming vector.

Complex Number Processing: Near-field channel state information is typically expressed in complex form, necessitating preprocessing to convert it into real numbers before feeding it into the neural network. Diverging from the conventional approach of concatenating real and imaginary parts into a one-dimensional vector, this paper adopts vertical stacking and utilizes a convolutional neural network for information extraction. The key benefit of this processing method is its ability to preserve the correlation information between the real and imaginary parts, particularly the phase information.

Unsupervised Learning Loss Function Definition: We try to find a codebook-independent beamforming scheme. The beamforming problem of design can be regarded as an unsupervised learning problem. In unsupervised learning, we define the negative value of the achievable rate as a loss function. By minimizing this loss function, the neural network will tend to increase the achievable rate of the system.

C. Our Contributions

To reduce the overhead of beam training, we proposed a near-field beamforming method based on deep learning. In this approach, a convolutional neural network architecture is designed to optimize beamforming according to the channel state information fed back by the receiver. The main contributions of this paper are as follows.

- We propose an XL-MIMO near-field beamforming algorithm based on unsupervised deep learning. Utilizing the estimated channel state information as input and the negative achievable rate as the loss function, the designed beamformers can directly produce the beamforming vector satisfying the modulus constraints.
- A convolutional neural network is designed to extract complex information effectively. After stacking the real part and the imaginary part, the correlation information (phase information) between the real part and the imaginary part is preserved through reasonable design padding and convolution kernel size.
- Numerous simulation experiments verify the effectiveness of the designed beamforming scheme. Compared with the traditional beamforming method, the experimental results show that the proposed method has significant advantages in improving the communication rate and reducing the computational complexity.

D. Organization and Notation

1) *Organization:* The structure of this paper is outlined as follows. In section II, we introduce the characteristics of near field propagation, near-field channel models, and near-field beamforming. Subsequently, section III provides an in-depth presentation of the near-field beamforming method based on deep learning. In section IV, we provide the experimental setup and performance analysis of the proposed scheme. Finally, section V provides a summary of the work.

2) *Notations:* Unless otherwise indicated, matrices are represented by bold capital letters (i.e. \mathbf{C}), vectors are denoted by

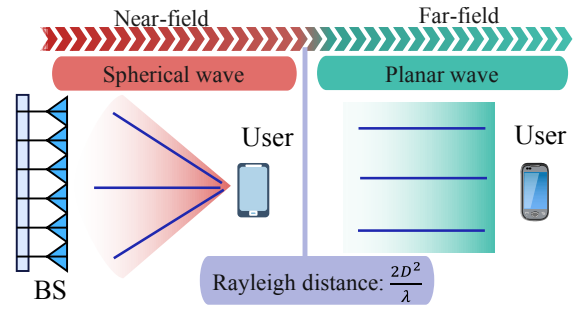


Fig. 1. Near-field wavefront and far-field wavefront comparison

bold lowercase letters (i.e. \mathbf{h}), and scalars are denoted by plain font (i.e. d). \mathbf{h}_k denotes the k -th element of the vector \mathbf{h} . \mathbf{w}^H denotes the conjugate transpose of the vector \mathbf{w} . $\mathcal{CN}(\mu, \sigma_n^2)$ denotes a complex Gaussian random distribution with mean μ and covariance σ_n^2 .

II. NEAR-FIELD COMMUNICATIONS SYSTEM MODEL

A. Near-field Propagation

In wireless communication, we typically delineate the division between the far field and near field using the Rayleigh distance expressed by the following [34].

$$RD = \frac{2D^2}{\lambda_c} = \frac{2D^2 f_c}{C}, \quad (1)$$

where D represents the antenna diameter, λ_c denotes the wavelength, f_c is the carrier center frequency, and C is the rate of light. As illustrated in Fig. 1, when the distance between the receiver and transmitter exceeds the Rayleigh distance, the transmission is classified as occurring in the far field. The propagation of electromagnetic waves in the far field can be simplified using a plane wave model. The area between the transmitter and RD is designated as the radiation near-field region. In the near field, signal propagation is influenced by the antenna and propagation distance, modeled as a spherical wave.

As indicated in Table I, with an antenna aperture of 0.5m and a carrier center frequency of 50MHz, any region beyond 0.09m from the BS is categorized as the far-field. Before the advent of the fifth generation (5G) of mobile communications, the near-field region is considerably restricted owing to the small antenna aperture and the utilization of low-frequency bands. Communication is typically perceived to predominantly occur in the far-field. However, with the widespread adoption of millimeter wave bands for 5G, especially when combined with relatively large antenna arrays, near-field distances can reach tens to hundreds of meters. For instance, in the 802.11ay communication protocols, the frequency band spans from 58.32 to 70.2 GHz. As clearly illustrated in Table I, when the carrier frequency is 60 GHz and the antenna diameter is $D=0.5$ meters, any UE within a distance less than 100 meters from the BS is considered to be in the near-field region. In this case, the approximation of the signal wavefront as a plane is no longer applicable, necessitating consideration of a spherical

wavefront. Consequently, it holds paramount significance to explore how to effectively harness this non-negligible spherical wavefront shape.

TABLE I
VARIATION IN THE NEAR-FIELD REGION WITH CARRIER CENTER FREQUENCIES.

Antenna diameter (D)	Center frequency (f_c)	Near-field Boundary
0.5m	50MHz	0.09m
0.5m	1000MHz	1.7m
0.5m	5GHz(802.11a)	8.3m
0.5m	28GHz	47m
0.5m	60GHz(802.11ay)	100m

B. Near-field Channel Model

In this paper, we investigate downlink beam training for broadband extremely large-scale multiple-input-multiple-output(XL-MIMO) systems. The BS is equipped with a uniform linear array (ULA) with N transmitting antennas and utilizes orthogonal frequency division multiplexing (OFDM) to serve multiple omnidirectional antennas UEs. We assume that the BS has N_t antennas with an antenna spacing of $d = \lambda_c/2$. Let M denote the number of subcarriers in OFDM, B represent the system bandwidth, and f_c represent the center carrier frequency. The frequency of subcarrier m is determined as $f_m = f_c + \frac{B(2m-1-m)}{2M}$, $\forall m \in M = \{1, \dots, M\}$. Given the predominant reliance of mmWave communications on line-of-sight links (LOS), we consider a single LOS radio frequency (RF) chain. Our focus is on beam training for downlink multi-user systems.

To emphasize the distinctions between near-field and far-field channel models, we initially introduce the far-field channel model, a prevalent consideration in current research. As depicted in green in Fig. 2, the far-field signal exhibits a plane wavefront. Assuming the distance from the central antenna to the UE is r , the distance between the UE and antenna n is:

$$r_n^{far} = r - nd \sin \theta. \quad (2)$$

The m -th subcarrier downlink channel between the n -th antenna and the UE can be represented as:

$$h_{n,m}^{far} = g_n e^{-j \frac{2\pi f_m}{c} r_n^{far}} = \tilde{g}_n e^{-j \frac{2\pi f_m}{c} nd \sin \theta}, \quad (3)$$

where g_n is the channel gain, $\tilde{g}_n = g_n e^{-j \frac{2\pi}{\lambda_m} r}$ is the equivalent channel gain. For broadband systems, we compute the guidance vector solely based on the center carrier frequency. The far-field channel steering vector can be expressed as:

$$\mathbf{b}^{far}(\theta) = \left[e^{-j \frac{2\pi f_c}{c} \frac{N}{2} d \cos \theta}, \dots, e^{j \frac{2\pi f_c}{c} nd \sin \theta}, \dots, e^{j \frac{2\pi f_c}{c} \frac{N}{2} d \sin \theta} \right]^T. \quad (4)$$

It can be observed that the far-field antenna response is a function of θ and is independent of the UE's distance r from the antenna.

As indicated by the red region in Fig. 2, when the distance between the antenna array and the receiver is less than RD ,

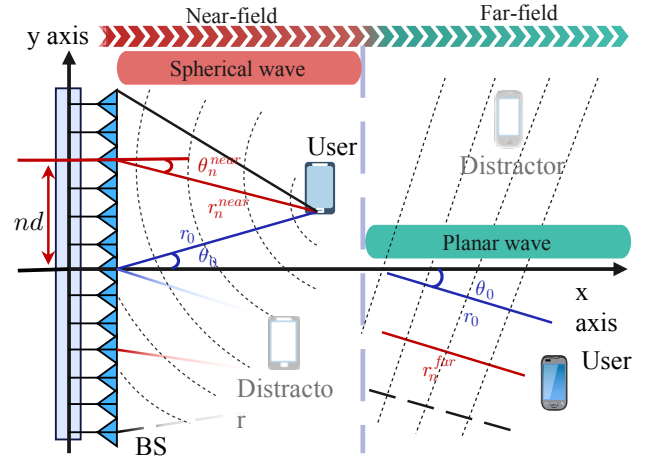


Fig. 2. Near-field and far-field channel model between BS and UE

the receiver is situated in the near-field region. Considering the property of the near-field spherical wave, the distance between the UE and antenna n is:

$$r_n^{near} = \sqrt{r^2 + n^2 d^2 - 2rnd \sin \theta}. \quad (5)$$

Then, the baseband frequency domain channel between the n -th antenna unit with a subcarrier frequency of f_m and the UE is expressed by the following formula:

$$h_{n,m}^{near} = \beta_n e^{-j \frac{2\pi f_m}{c} (\sqrt{r^2 + n^2 d^2 - 2rnd \cos \theta} - r)}. \quad (6)$$

By stacking the channels of all antenna units into one vector, the overall near-field channel for k -th UE can be obtained:

$$\mathbf{h}_k^{near} = \left[\sum_{i=1}^m h_{1,i}^{near}, \sum_{i=1}^m h_{2,i}^{near}, \dots, \sum_{i=1}^m h_{n,i}^{near} \right]. \quad (7)$$

It can be observed that the near-field antenna response is a function of the angle θ and the distance r , and there is no univariate linear correlation. Based on this, we can represent the near-field steering vector as:

$$\mathbf{b}^{near}(r, \theta) = \left[e^{-j \frac{2\pi f_c}{c} (r_n^{near} - r)}, \dots, e^{j \frac{2\pi f_c}{c} (r_n^{near} - r)}, \dots, e^{j \frac{2\pi f_c}{c} (r_n^{near} - r)} \right]^T. \quad (8)$$

This paper focuses on near-field beamforming. For simplicity, the superscript "near" in near-field parameters will be omitted below. The received signal of the downlink for the k -th UE can be expressed as:

$$y_k = \sqrt{G} \mathbf{w}^H \mathbf{h}_k s + n, \quad (9)$$

where G represents transmitting antenna power, \mathbf{w} represents the beamforming vector, \mathbf{h}_k represents the channel between BS and k -th UE, and s is the downlink transmit signal. $n \sim \mathcal{CN}(0, \sigma_n^2)$ represents the additive white Gaussian noise (AWGN) vector. The objective of our beamforming scheme is to maximize achievable rate of the target UE and minimize interference. For instance, when transmitting signals to UE 1, the signals received by UE 2 and UE 3 is considered

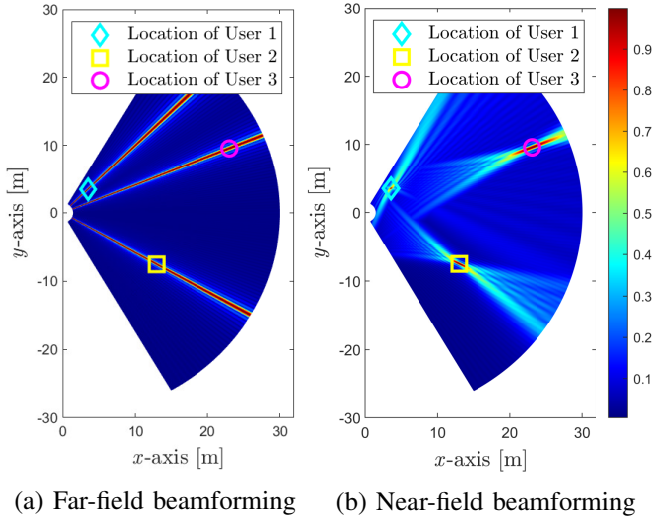


Fig. 3. (a) represents the standardized signal energy obtained by the receiver through far-field beam focusing, and (b) represents the standardized signal energy obtained by the receiver through near-field beam focusing. The far-field beam travels in different directions, while the near-field beam splitter focuses the beam at different locations.

interference. Assuming that the sent signal is $|s|^2 = 1$, the achievable rate of the m -th UE can be expressed as:

$$R_k = \log_2 \left(1 + \frac{G |\mathbf{w}^H \mathbf{h}_k|^2}{\sum_{i \neq m} |\mathbf{w}^H \mathbf{h}_i|^2 + \sigma_n^2} \right). \quad (10)$$

In the above formula, we consider UE interference as noise.

C. Near-field Beamforming

Since the far-field antenna response is solely dependent on the angle, the far-field beamforming only requires searching in the angular domain. As depicted in Fig. 3(a), one sector-shaped area can be covered per search. Consequently, this approach introduces significant interference for collinear UEs, those at different distances but the same angle. In contrast, the near-field antenna response is not only angle-dependent but also distance-dependent, enabling us to mitigate interference for collinear UEs. As illustrated in Fig. 3(b), the near-field beam focuses not on a specific angular domain but on the UE's location, substantially enhancing the received signal power. However, this advantage comes with the challenge that the near-field codebooks demand more codewords than the far-field codebook. Addressing the challenge of elevated training costs associated with complex codebooks is one of the primary objectives of this study.

We presume the utilization of a predefined codebook for beamforming. Considering that the steering vector in the near-field is influenced by both angle and distance, the angular domain Discrete Fourier Transform (DFT) codebook utilized in the far-field domain becomes obsolete. Upon incorporating distance sampling, the codebook in the polar coordinate

domain is expressed as:

$$\begin{aligned} \mathcal{W} = \{ & \mathbf{b}(\theta_1, r_1), \dots, \mathbf{b}(\theta_1, r_j), \dots, \mathbf{b}(\theta_1, r_J), \\ & \dots \\ & \mathbf{b}(\theta_i, r_1), \dots, \mathbf{b}(\theta_i, r_j), \dots, \mathbf{b}(\theta_i, r_J), \\ & \dots \\ & \mathbf{b}(\theta_I, r_1), \dots, \mathbf{b}(\theta_I, r_j), \dots, \mathbf{b}(\theta_I, r_J) \}, \end{aligned} \quad (11)$$

where each element represents a candidate beam code word, θ_i denotes the i -th sampling angle, and r_j denotes the j -th sampling distance. Our objective is to optimize the selection of codewords from a predefined codebook to maximize the achievable data rate. The pertinent problem of code word selection can be formulated as:

$$\mathbf{w}^* = \arg \max_{\mathbf{w} \in \mathcal{W}} \log_2 \left(1 + \frac{P |\mathbf{h} \mathbf{w}|^2}{\sum_{i \neq m} |\mathbf{w}^H \mathbf{h}_i|^2 + \sigma_n^2} \right). \quad (12)$$

The most straightforward approach to address the aforementioned challenges is through exhaustive beam scanning, aiming to find the optimal beam configuration that maximizes the achievable data transfer rate. However, compared to far-field scenarios, this method may incur unacceptable training costs, especially in mmWave communications, where higher frequencies and increased signal blockage lead to elevated path losses. Moreover, the nonlinear distance information in the near-field channel further complicates beam training, making traditional methods challenging for accurate modeling.

Given the outstanding performance of deep learning in handling complex nonlinear problems, particularly when trained on large-scale datasets, it has proven effective in uncovering intricate patterns hidden within the data. In the next section, we will explore how to leverage deep learning techniques, specifically neural networks, to accomplish beam training in near-field channels. Through deep learning, our aim is to more effectively capture the nonlinear characteristics of the channel, thereby reducing the computational and communication overhead associated with beam training.

III. DEEP LEARNING BASED NEAR-FIELD BEAMFORMING METHOD

A. Problem Formulation

The near-field codebook typically experiences a significant size due to the close correlation between the near-field channel and both angle and distance information. This introduces substantial computational complexity when employing codebook-based beam design. In practical scenarios, our primary focus is on the beam gain directed towards the target UE's location, rather than optimizing the beam gain for every grid across the entire space. Our objective is to achieve effective control over the beamforming shape without relying on a predefined codebook, aiming to maximize the achievable data transfer rate. Considering the constant modulus constraint $\|w_i\|^2 = 1$, for $i = 1, \dots, N_t$, the optimization problem concerning the beamforming vector \mathbf{w} is given by the following formula:

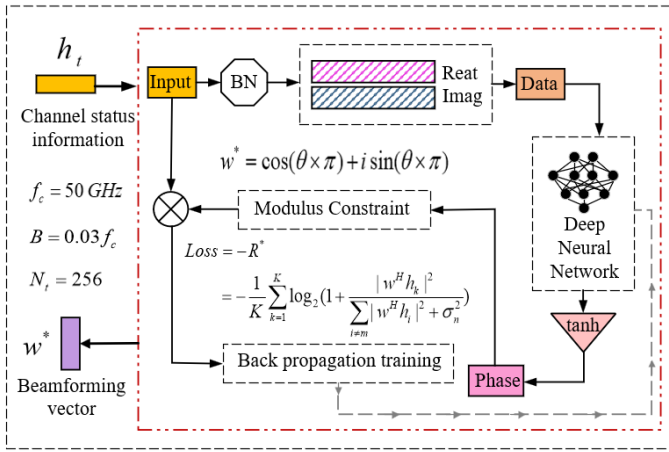


Fig. 4. Overall architecture diagram of the proposed model. This shows how to obtain the beamforming vector by using neural network when the channel state information is available.

$$\begin{aligned} \max_{\{w\}} \quad & \sum_{k=1}^K R_k(w) \\ \text{s.t.} \quad & w_i \in \mathbf{w} \\ & |w_i|^2 = 1, \forall i \in N_t. \end{aligned} \quad (13)$$

The channel state information in XL-MIMO systems is intricate, giving rise to the nonlinearity and significant non-convexity of the aforementioned challenges.

We introduce deep learning as a powerful tool to address these issues. In this paper, a unsupervised learning of neural networks model is designed to enable beamforming vectors to adapt and learn flexibly under complex channel conditions. Our goal is to find the mapping function Φ_ξ of parameter ξ , which uses CSI to predict the best beamforming vectors w . The mapping function can be expressed as:

$$\Phi_\xi\{h\} \rightarrow \{\hat{w}\}, \quad (14)$$

where h denotes the downlink channel state information from the BS to the UE, and \hat{w} represents the desired beamforming vector. It should be noted that the process of obtaining \hat{w} from h is quite complicated.

B. Deep Learning Scheme Design

The overall architecture of our proposed model is shown in Fig. 4. The channel sample h generated by the simulation is input into the neural network. Subsequently, the neural network iteratively learns the model parameters through gradient descent to minimize the predefined loss function. By adjusting the learning rate, we can converge the model to an approximate global optimal solution.

Once the model is trained, all parameters of the network ξ will be fixed. In online deployment, we only need to input the channel status information h , and the network will directly output the beamforming vector w . Algorithm 1 shows the pseudo-code of our proposed scheme. In the design of the

network structure, we introduce some innovative mechanisms to ensure the effectiveness of the designed scheme.

Algorithm 1: Unsupervised Deep Learning for Near-field Beamforming

- Input:** Channel state information h .
Output: Beamforming vector \hat{w} .
- 1 **Initialize:** The number of UEs K ; SNR; The number of transmit antennas N_t ; The normalized transmit power P ;
 - 2 Calculate the input h of neural network according to formula 7. **Train the Neural Network;**
 - 3 **for** $epoch \leftarrow 1$ to E **do**
 - 4 Randomly sample a batch of training data (h, SNR) ;
 - 5 Calculate the output of the neural network θ ;
 - 6 Calculate the phase $\theta \leftarrow \pi\theta$;
 - 7 Calculate the complex beamforming vector according to formula 16;
 - 8 Calculate the loss according to formula 17;
 - 9 Update the neural network parameters using backpropagation: $\xi \leftarrow \xi - \eta \cdot \nabla_\xi \text{loss}$;
 - 10 **end**
 - 11 **Inference;**
 - 12 Given new channel state information h_{new} ;
 - 13 Calculate the beamforming vector $\hat{w} = \cos(\pi\theta) + j \cdot \sin(\pi\theta)$;
-

1) Input Data Generation: Each simulation generates positions for K UEs at T time frames, all of which fall within the specified Angle and distance sampling range. When the BS provides service to UE k , the remaining $K-1$ UEs are considered interference, which will be reflected in the loss function we design. The channel sample h generated by the system model presented in Section 3 is used as input data. Detailed parameter design is shown in Table II.

TABLE II
COMMUNICATION SYSTEM SIMULATION PARAMETERS.

Parameter	Symbol	Value
Number of Transmit Antennas	N_t	256
Number of Receive Antennas	N_r	1
Signal Noise Ratio	SNR	[-20dB, 20dB]
Sampling Distance	R	[5m, 50m]
Sampling Angle	θ	[-60°, 60°]
Center Carrier Frequency	f_c	50GHz
Bandwidth	B	1.5GHz
Number of Carriers	M	128
Number of UEs	K	3
Time Frame	T	10000

2) Complex Number Feature Extraction: Different from previous approaches that solely rely on multi-layer fully connected methods, we leverage convolutional neural networks for the intricate task of extracting features from complex signals. The input data dimension is $2 \times N_t$, and we transform it into

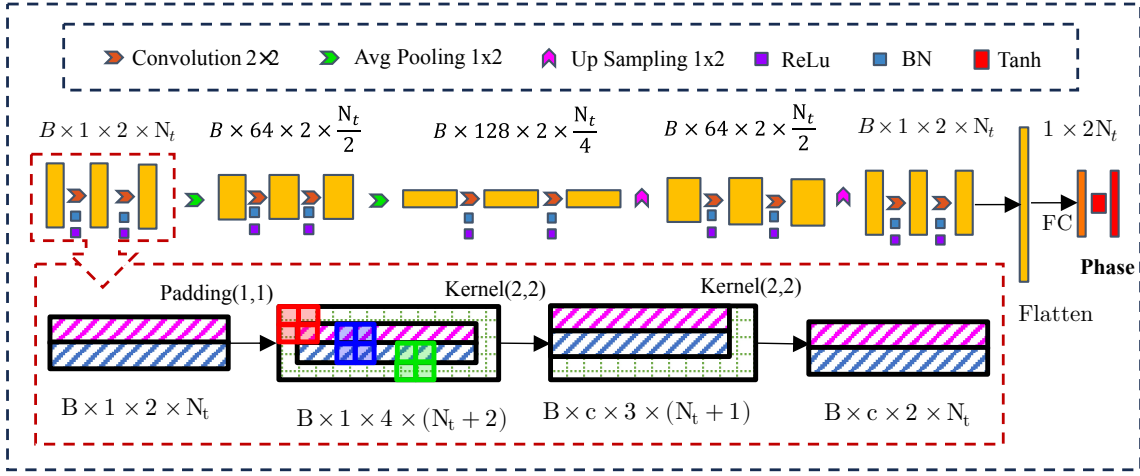


Fig. 5. Illustrate the structure of the convolutional neural network design. The red dotted boxes depict the intricate details of feature extraction for the aforementioned complex data. The orange rectangle represents the data transformations within the convolutional neural network, and the red rectangle highlights the process of obtaining the desired phase θ .

$1 \times 2 \times N_t$ by adding an extra dimension. The structure is shown in Fig. 5, the orange rectangles depict the layers of our model. Each set of three identically sized rectangular blocks is termed a feature extraction block. Within this block, the data undergoes two convolution layers, a regularization layer (BatchNorm), and an activation layer (ReLU).

With meticulously designed padding and convolution kernel size, we ensure that the data size remains unchanged before and after passing through the feature extraction block, as outlined in the red dashed box. Initially, the input data of $B \times 1 \times 2 \times N_t$ is transformed to $B \times 1 \times 4 \times (N_t + 2)$ by introducing padding, followed by a 2×2 convolution operation. In the convolution process, the red position of the kernel extracts real part information, the blue position captures information combining real and imaginary parts, and the green position extracts imaginary part information. After the initial convolution operation, the data size becomes $B \times 1 \times 3 \times (N_t + 1)$. Subsequent convolution restores the data size to $B \times 1 \times 2 \times N_t$, aligning with the dimensions of the input data.

After the data undergoes a feature extraction block, we employ average pooling for downsampling. At this point, the channel count increases, and the data length is halved compared to the original. After repeating this process twice, the data size becomes $B \times c \times 2 \times N_t/4$, where c is the number of channels. Subsequently, the data undergoes deconvolution and a feature extraction block, where the channel count is reduced, and the data length is doubled. After repeating this procedure twice, the data size becomes $B \times 1 \times 2 \times N_t$, matching the dimensions of the input data. The utilization of a convolutional neural network not only allows for the extraction of more diverse data features but also significantly reduces the model's complexity. The analysis of model complexity is presented in the following section.

3) Convert Angles into Beamforming Vectors: In the left end of Fig. 5, after the feature extraction block fully captures the features, the data is flattened into a one-dimensional vector. The data size becomes $1 \times N_t$ following a fully connected layer. To ensure that the neural network's output is a complex-

valued vector adhering to the norm constraint, a "tanh" layer is introduced at the final layer of the network. Specifically, its output is a real value denoted as θ , and after passing through the "tanh" activation layer, its value is confined to the range $(0, 1)$. Multiplying the output by π yields the phase within the range of $[-\pi, \pi]$. The mathematical expression for this process is as follows:

$$\begin{aligned} \text{Phase} : \theta &\in [-1, 1] \\ \theta \times \pi &\in [-\pi, \pi]. \end{aligned} \quad (15)$$

Then, Euler's formula is applied to convert the phase into the desired complex-valued beamforming vector, with the complex output given by the following formula:

$$w = \exp(j \cdot \pi) = \cos(\pi\theta) + j \cdot \sin(\pi\theta), \quad (16)$$

where $j = \sqrt{-1}$. It can be observed that $\theta\pi$ has a clear physical meaning, with its elements corresponding to the equivalent phases of the beamforming coefficients in w .

4) Loss Function Design: We adopt an unsupervised learning approach, where the neural network is guided by a loss function directly linked to the beamforming target. The loss function for the task is defined as the negative of the average achievable rate.

$$\begin{aligned} \text{Loss} &= -\frac{1}{Q} \sum_{q=1}^Q R^* \\ &= -\frac{1}{QK} \sum_{q=1}^Q \sum_{k=1}^K \log_2 \left(1 + \frac{|w^H h_k|^2}{\sum_{i \neq m} |w^H h_i|^2 + \sigma_n^2} \right) \end{aligned} \quad (17)$$

Where Q represents the total number of training samples and k represents the number of UEs. σ_n^2 , h_k , and w represent the SNR, CSI, and the output analog beamforming vector associated with the K th sample, respectively. It should be emphasized that the decrease in loss directly corresponds to the increase in the average achievable rate.

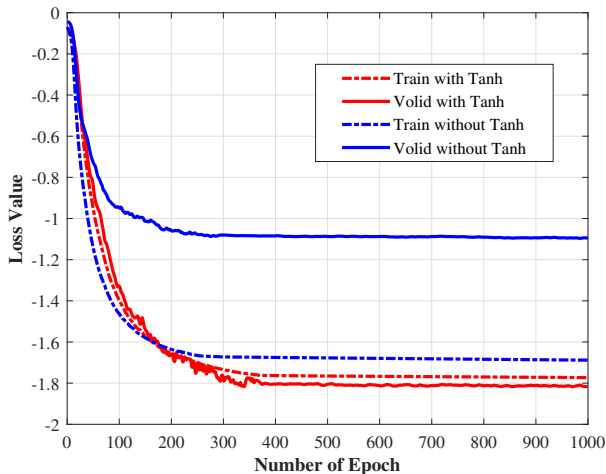


Fig. 6. Training loss curves of models with and without Tanh layer

IV. EXPERIMENTAL SETUP AND SIMULATION ANALYSIS

A. Experimental Setup

TABLE III
SIMULATION EXPERIMENT HYPERPARAMETER CONFIGURATION

Hyperparameter	Value
Initial Learning Rate	10^{-2}
Batch Size	256
Number of Epoch	10000
Convolution Kernel Size	(2,2)
Optimizer	Adam

In the proposed unsupervised deep learning model, the hyperparameter Settings are shown in Table III. The data set is randomly divided into a 75% training set and a 25% test set. The learning rate is initialized to 10^{-2} and dynamically decreases when the evaluation metric no longer improved. Parameter tuning is conducted using the Adam optimizer, with a batch size set to 256.

We utilize Python as the programming language to construct the deep learning network model using the PyTorch framework. The experimental system environment comprises Ubuntu 16.04, Python 3.9, and PyTorch 1.1. The graphics card employed is an NVIDIA GeForce RTX 3060 12GB GPU.

B. Experimental Result

During the simulation experiment, a evenly spaced half-wave linear array with $N_t = 256$ was deployed at BS. The simulation parameters align with the millimeter-wave near-field channel model outlined in Section 3. The results of the proposed scheme compared with the baseline scheme [35], [36] are as follows, with the average achievable rate defined as the evaluation indicator.

The model training loss curve is presented in Fig. 6 to validate its effective convergence. The four curves depict the loss evolution of the training set and the validation set with

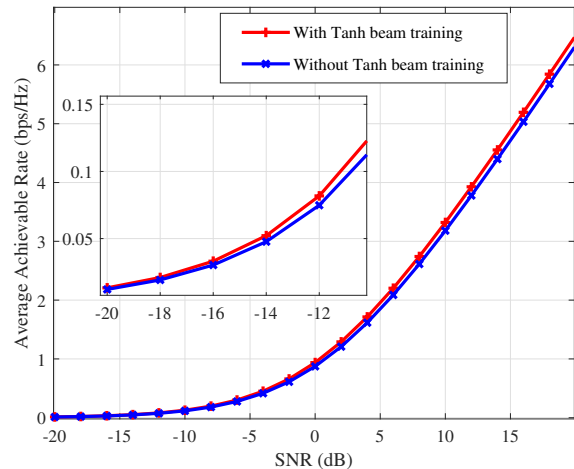


Fig. 7. Comparison of beamforming effects with and without Tanh layer

the tanh layer, and the loss changes of the training set and the validation set without the tanh layer, respectively. It can be observed that models with tanh layers exhibit superior performance, with lower loss values, and also better performance on verification sets. Conversely, models without tanh layers exhibit pronounced overfitting. This confirms that the incorporation of the tanh layer to confine the phase within the range $[-1, 1]$ enhances the nonlinearity of the model and effectively mitigates overfitting.

We rigorously examine whether the inclusion of the tanh layer can enhance the beamforming performance. Fig. 7 illustrates the average achievable rate associated with the beamforming vector output by the model before and after the addition of the tanh layer. The results show that for all SNR values, the model with tanh layer achieves a higher average achievable rate than the model without tanh layer. And this improvement becomes more pronounced with increasing SNR.

Fig. 8 shows the variation in the average achievable rate with the SNR under different beam training schemes, where SNR increases from -20dB to 20dB. The graph clearly demonstrates that the proposed scheme consistently outperforms existing far-field and near-field beam training schemes across a wide range of SNR values. When SNR = 20dB, our proposed scheme achieves an approximately 18%, 30%, and 120% improvement in average achievable rate compared to the near-field hierarchical beamforming scheme, far-field hierarchical scheme, and exhaustive search scheme, respectively. Notably, when the SNR > -5 dB, the scheme shows obvious performance gain compared with the comparison scheme. Furthermore, the proposed scheme does not exhibit clear superiority at low SNR. Under low SNR conditions, where noise power surpasses signal power, neural networks struggle to effectively extract signal features. Our scheme might be vulnerable to noise under conditions of low SNR. Investigating potential solutions to mitigate noise sensitivity represents a focal point for our future research efforts.

With the expanding communication frequency band, carrier frequency has emerged as a crucial factor influencing commu-

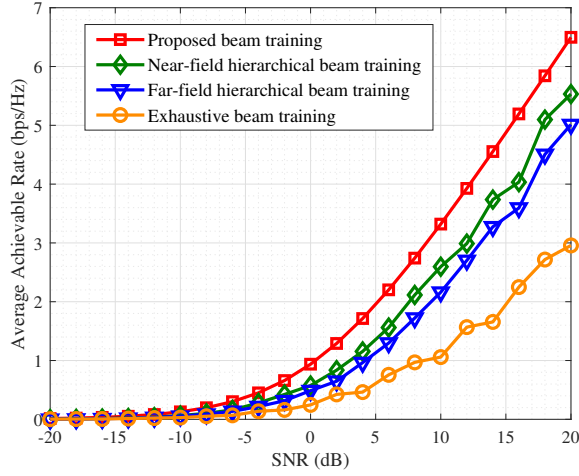


Fig. 8. The variation curve of the average achievable rate of different schemes with SNR.

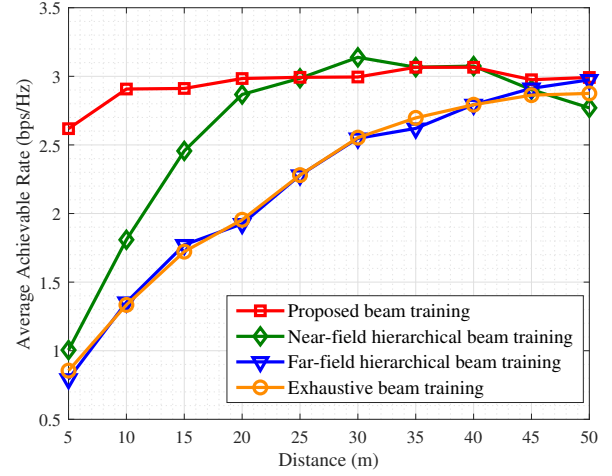


Fig. 10. Average achievable rate curves at different distance.

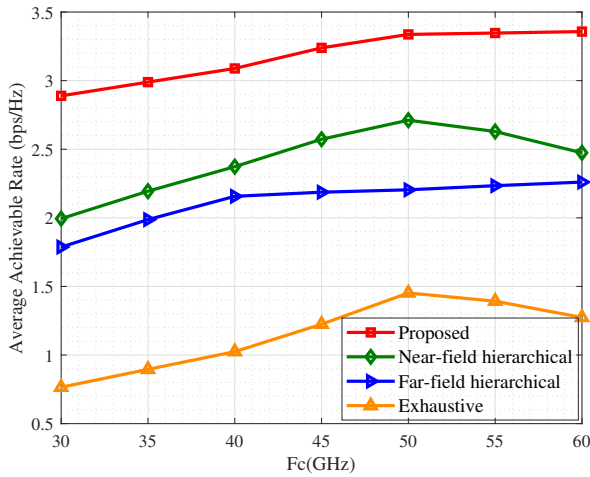


Fig. 9. The average achievable rate varies with the central carrier frequency.

nication rates. Illustrated in Fig. 9 are the average achievable rate curves for the proposed scheme and the comparative scheme at different central carrier frequencies. In this context, the SNR is set to 10dB, and UE’s positions and angles align with the specifications outlined in Table II. The figure distinctly illustrates that for all carrier frequencies, our proposed scheme consistently outperforms other schemes in terms of average achievable rates. For the far-field hierarchical scheme, with the increase of carrier frequency, near-field propagation gradually dominates, resulting in that the average achievable rate of the far-field scheme basically no longer increases when the carrier is greater than 40GHz. Optimal performance for all solutions is observed at a carrier frequency of 50GHz. This is attributed to the increased free-space propagation losses incurred by high-frequency signals during transmission. As the carrier frequency rises, the performance gain achieved by augmenting the number of antennas becomes insufficient to counterbalance the escalating free-space propagation losses. Notably, when $f_c > 50\text{GHz}$, the comparative scheme experiences a decline

in performance, whereas the proposed scheme’s performance remains relatively stable, affirming the robustness of our proposed solution. Given the constraint of restricting the training cost for the exhaustive search scheme to 256, the scheme encounters challenges in conducting precise searches in high-frequency bands, leading to a notable degradation in performance.

Fig. 10 illustrates the correlation between the average achievable rate and the UE-to-BS distance. Here, the distance r from the UE to the BS gradually increases from 5 meters to 50 meters. The SNR is set to 10dB, the UE’s angle θ is set $[-60^\circ, 60^\circ]$, and the carrier frequency is set to 50GHz. Other simulation parameters are consistent with those in Table II. The observations in Fig. 10 reveal the substantial impact of near-field propagation on beam training performance. Notably, when the UE is in close proximity to the BS, our proposed scheme exhibits superior rate performance compared to all the schemes under consideration. However, as the distance between the UE and the BS increases, the performance degradation of our scheme becomes comparable to that of the far-field hierarchical beam training scheme. For far-field schemes, the dominance of near-field propagation as the distance decreases leads to a rapid decline in the average rate of far-field schemes. Due to the limitation of the maximum training cost, the exhaustive scheme experiences severe degradation in the near-field region, impeding effective search for near-field positions. Additionally, the near-field hierarchical beam training scheme can moderately alleviate the decline in the average achievable rate, but its performance gradually diminishes when the distance exceeds 30 meters. Furthermore, when the distance is less than 20 meters, its performance notably lags behind the proposed scheme. In contrast, the proposed scheme demonstrates the ability to search for the optimal beamforming vector with minimal pilot overhead. This affirms the robustness of the proposed scheme in both near and far-field communications scenarios.

Fig.11 depicts the variation in average achievable rate with angle θ . Here, θ gradually increases from -60° to 60° , and the

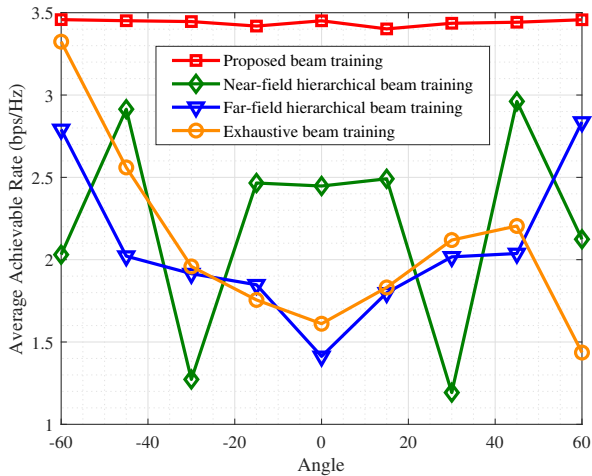


Fig. 11. Average achievable rate curves at different angles.

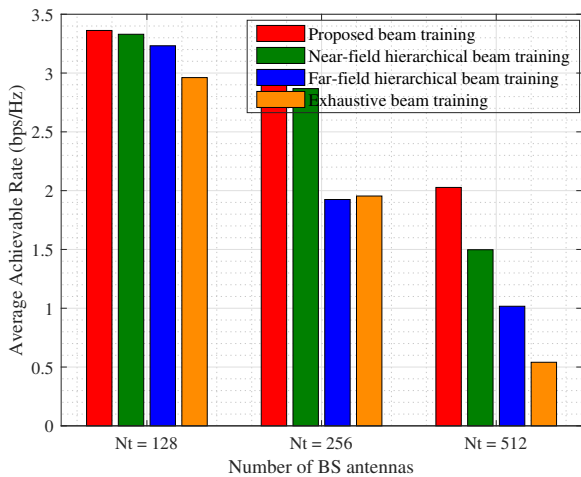


Fig. 12. Impact of transmitting antenna quantity on beamforming performance.

distance (r) is randomly generated within the range [5m, 50m]. The SNR is set to 10 dB, and the remaining simulation settings mirror those in Table II. Notably, for the far-field scheme, performance degrades significantly as θ approaches 0. This degradation is attributed to the increased prominence of near-field effects near zero angles, which has been demonstrated in the literature [37]. Furthermore, the near-field hierarchical beam training scheme exhibits noticeable fluctuations. This is because the near-field mixing scheme creates a near-field codebook by uniformly sampling angles and distances in Cartesian coordinates. This approach proves challenging in achieving stable beamforming performance across the entire near-field environment [30]. In contrast, our proposed scheme consistently attains the highest average achievable rate across all considered angles. This result underscores the robustness and effectiveness of our approach in handling the challenges posed by varying angles in near-field communications scenarios.

Fig. 12 illustrates the average achievable rates by various schemes under different number of BS antennas N_t . In this

experiment, The SNR is set to 10 dB, and other simulation parameters remained consistent with those in Table II. From the observation results, with the increase of the number of antennas, all schemes face a trend of performance degradation. Remarkably, our proposed scheme consistently exhibits superior performance compared to all comparison schemes. With the growth in the number of antennas, the performance of the proposed model improves more significantly than that of the comparison model. The escalating number of antennas makes it more difficult for traditional schemes to deal with intricate beam codebooks. This further substantiates the exceptional robustness and resilience of our proposed scheme under diverse conditions. The consistent outperformance of our model in the face of increasing antenna numbers underscores its adaptability and suitability for evolving communication scenarios.

V. CONCLUSIONS

In this paper, we proposed a near-field beamforming scheme based on unsupervised deep learning. By skillfully designing the padding and kernel size of the convolutional neural network, we effectively extract the features of the complex channel state information. During the network training process, we utilize the negative value of the total achievable rate in the multi-user network as the loss function and ensure the amplitude constraint of the beamforming vector through a customized Tanh layer. Our solution doesn't rely on a predefined codebook and only requires the estimated channel state information as input to obtain the optimal beamforming vector. Simulation results demonstrate the competitive performance of the proposed scheme.

REFERENCES

- [1] W. Saad, M. Bennis, and M. Chen, "A Vision of 6G Wireless Systems: Applications, Trends, Technologies, and Open Research Problems," *IEEE Network*, vol. 34, no. 3, June 2020, pp. 134–42.
- [2] B. Rong, "6G: The Next Horizon: From Connected People and Things to Connected Intelligence," in *IEEE Wireless Communications*, vol. 28, no. 5, pp. 8-8, October 2021, doi: 10.1109/MWC.2021.9615100.
- [3] "6G: The next horizon white paper," Huawei, Jun. 2022. [Online]. Available: <https://www.huawei.com/en/huaweitech/future-technologies/6g-white-paper>
- [4] H. Lu and Y. Zeng, "Communicating With Extremely Large-Scale Array/Surface: Unified Modeling and Performance Analysis," in *IEEE Transactions on Wireless Communications*, vol. 21, no. 6, pp. 4039-4053, June 2022, doi: 10.1109/TWC.2021.3126384.
- [5] Z. Zhang, Y. Xiao, Z. Ma, M. Xiao, Z. Ding, X. Lei, G. K. Karagiannidis, and P. Fan, "6G wireless networks: Vision, requirements, architecture, and key technologies," *IEEE Veh. Technol. Mag.*, vol. 14, no. 3, pp. 28–41, Sep. 2019.
- [6] E. Björnson, L. Sanguinetti, H. Wymeersch, J. Hoydis, and T. L. Marzetta, "Massive MIMO is a reality—What is next?: Five promising research directions for antenna arrays," *Digital Signal Process.*, vol. 94, pp. 3–20, Nov. 2019.
- [7] X. Wu, J. Sun, X. Jia and S. Wang, "Source Localization for Extremely Large-Scale Antenna Arrays with Spatial Non-Stationarity," *ICASSP 2023 - 2023 IEEE International Conference on Acoustics, Speech and Signal Processing (ICASSP)*, Rhodes Island, Greece, 2023, pp. 1-5, doi: 10.1109/ICASSP49357.2023.10095886.
- [8] K. T. Selvan and R. Janaswamy, "Fraunhofer and Fresnel Distances: Unified derivation for aperture antennas," in *IEEE Antennas and Propagation Magazine*, vol. 59, no. 4, pp. 12-15, Aug. 2017, doi: 10.1109/MAP.2017.2706648.
- [9] X. Li, H. Lu, Y. Zeng, S. Jin and R. Zhang, "Near-Field Modeling and Performance Analysis of Modular Extremely Large-Scale Array Communications," in *IEEE Communications Letters*, vol. 26, no. 7, pp. 1529-1533, July 2022, doi: 10.1109/LCOMM.2022.3172437.

- [10] C. Poongodi, D. Deepa, K. Shoukath Ali, D. Muthumanickam and T. Perarasi, "Channel Estimation of XL-MIMO in 6G Communication System - Near Field Analysis," 2023 Third International Conference on Smart Technologies, Communication and Robotics (STCR), Sathyamangalam, India, 2023, pp. 1-4, doi: 10.1109/STCR59085.2023.10396963.
- [11] Y. Liu, J. Xu, Z. Wang, X. Mu and Hanzo, L.H. (2023). Near-Field Communications: What Will Be Different? ArXiv, abs/2303.04003.
- [12] Y. Zhang, X. Wu and C. You, "Fast Near-Field Beam Training for Extremely Large-Scale Array," in IEEE Wireless Communications Letters, vol. 11, no. 12, pp. 2625-2629, Dec. 2022, doi: 10.1109/LWC.2022.3212344.
- [13] Y. Liu, Z. Wang, J. Xu, C. Ouyang, X. Mu and R. Schober, "Near-Field Communications: A Tutorial Review," in IEEE Open Journal of the Communications Society, vol. 4, pp. 1999-2049, 2023, doi: 10.1109/OJCOMS.2023.3305583.
- [14] Z. Wu and L. Dai, "Multiple Access for Near-Field Communications: SDMA or LDMA?," in IEEE Journal on Selected Areas in Communications, vol. 41, no. 6, pp. 1918-1935, June 2023, doi: 10.1109/JSAC.2023.3275616.
- [15] M. Cui, Z. Wu, Y. Lu, X. Wei and L. Dai, "Near-Field MIMO Communications for 6G: Fundamentals, Challenges, Potentials, and Future Directions," in IEEE Communications Magazine, vol. 61, no. 1, pp. 40-46, January 2023, doi: 10.1109/MCOM.004.2200136.
- [16] S. Payami, M. Sellathurai and K. Nikitopoulos, "Low-Complexity Hybrid Beamforming for Massive MIMO Systems in Frequency-Selective Channels," in IEEE Access, vol. 7, pp. 36195-36206, 2019, doi: 10.1109/ACCESS.2019.2905430.
- [17] N. J. Myers and R. W. Heath, "InFocus: A Spatial Coding Technique to Mitigate Misfocus in Near-Field LoS Beamforming," in IEEE Transactions on Wireless Communications, vol. 21, no. 4, pp. 2193-2209, April 2022, doi: 10.1109/TWC.2021.3110011.
- [18] D. Slepian, "Prolate spheroidal wave functions, fourier analysis, and uncertainty — V: the discrete case," in The Bell System Technical Journal, vol. 57, no. 5, pp. 1371-1430, May-June 1978, doi: 10.1002/j.1538-7305.1978.tb02104.x.
- [19] H. Zhang, N. Shlezinger, F. Guidi, D. Dardari and Y. C. Eldar, "6G Wireless Communications: From Far-Field Beam Steering to Near-Field Beam Focusing," in IEEE Communications Magazine, vol. 61, no. 4, pp. 72-77, April 2023, doi: 10.1109/MCOM.001.2200259.
- [20] H. Zhang, N. Shlezinger, F. Guidi, D. Dardari, M. F. Imani and Y. C. Eldar, "Beam Focusing for Near-Field Multiuser MIMO Communications," in IEEE Transactions on Wireless Communications, vol. 21, no. 9, pp. 7476-7490, Sept. 2022, doi: 10.1109/TWC.2022.3158894.
- [21] David A. B. Miller, "Waves, modes, communications, and optics: a tutorial," Adv. Opt. Photon. 11, 679-825 (2019)
- [22] N. Decarli and D. Dardari, "Communication Modes With Large Intelligent Surfaces in the Near Field," in IEEE Access, vol. 9, pp. 165648-165666, 2021, doi: 10.1109/ACCESS.2021.3133707.
- [23] Z. Wang, X. Mu and Y. Liu, "Near-Field Integrated Sensing and Communications," in IEEE Communications Letters, vol. 27, no. 8, pp. 2048-2052, Aug. 2023, doi: 10.1109/LCOMM.2023.3280132.
- [24] J. Zuo, X. Mu and Y. Liu, "Near-Field Non-Orthogonal Multiple Access Communications," GLOBECOM 2023 - 2023 IEEE Global Communications Conference, Kuala Lumpur, Malaysia, 2023, pp. 649-654, doi: 10.1109/GLOBECOM54140.2023.10437973.
- [25] Z. Zhang, Y. Liu, Z. Wang, X. Mu and J. Chen, "Physical Layer Security in Near-Field Communications," in IEEE Transactions on Vehicular Technology, doi: 10.1109/TVT.2024.3366115.
- [26] W. Wu, D. Liu, X. Hou and M. Liu, "Low-Complexity Beam Training for 5G Millimeter-Wave Massive MIMO Systems," in IEEE Transactions on Vehicular Technology, vol. 69, no. 1, pp. 361-376, Jan. 2020, doi: 10.1109/TVT.2019.2926430.
- [27] F. Sahrabi and W. Yu, "Hybrid Digital and Analog Beamforming Design for Large-Scale Antenna Arrays," in IEEE Journal of Selected Topics in Signal Processing, vol. 10, no. 3, pp. 501-513, April 2016, doi: 10.1109/JSTSP.2016.2520912.
- [28] Z. Xiao, T. He, P. Xia and X. -G. Xia, "Hierarchical Codebook Design for Beamforming Training in Millimeter-Wave Communication," in IEEE Transactions on Wireless Communications, vol. 15, no. 5, pp. 3380-3392, May 2016, doi: 10.1109/TWC.2016.2520930.
- [29] H. Yu, P. Guan, W. Qu and Y. Zhao, "An Improved Beam Training Scheme Under Hierarchical Codebook," in IEEE Access, vol. 8, pp. 53627-53635, 2020, doi: 10.1109/ACCESS.2020.2981479.
- [30] M. Cui and L. Dai, "Channel Estimation for Extremely Large-Scale MIMO: Far-Field or Near-Field?," in IEEE Transactions on Communications, vol. 70, no. 4, pp. 2663-2677, April 2022, doi: 10.1109/TCOMM.2022.3146400.
- [31] C. Wu, C. You, Y. Liu, L. Chen and S. Shi, "Two-Stage Hierarchical Beam Training for Near-Field Communications," in IEEE Transactions on Vehicular Technology, vol. 73, no. 2, pp. 2032-2044, Feb. 2024, doi: 10.1109/TVT.2023.3311868.
- [32] M. Cui, L. Dai, Z. Wang, S. Zhou and N. Ge, "Near-Field Rainbow: Wideband Beam Training for XL-MIMO," in IEEE Transactions on Wireless Communications, vol. 22, no. 6, pp. 3899-3912, June 2023, doi: 10.1109/TWC.2022.3222198.
- [33] G. Jiang and C. Qi, "Near-Field Beam Training Based on Deep Learning for Extremely Large-Scale MIMO," in IEEE Communications Letters, vol. 27, no. 8, pp. 2063-2067, Aug. 2023, doi: 10.1109/LCOMM.2023.3289513.
- [34] J. D. Kraus and R. J. Marhefka, Antennas for all applications. New York, NY, USA: McGraw-Hill, 2002.
- [35] X. Wei, L. Dai, Y. Zhao, G. Yu, and X. Duan, "Codebook design and beam training for extremely large-scale RIS: Far-field or near-field?" China Commun., vol. 19, no. 6, pp. 193204, Jun. 2022.
- [36] S. Noh, M. D. Zoltowski, and D. J. Love, "Multi-resolution codebook and adaptive beamforming sequence design for millimeter wave beam alignment," IEEE Trans. Wireless Commun., vol. 16, no. 9, pp. 5689-5701, Sep. 2017.
- [37] M. Cui, L. Dai, R. Schober, and L. Hanzo, "Near-field wideband beamforming for extremely large antenna arrays," 2021, arXiv:2109.10054.



Jiali Nie is currently studying for a master's degree in the Beijing University of Posts and Telecommunications (BUPT), Beijing 100876, China. Her main research interests include wireless communication, integrated sensing and communication (ISAC), intelligent signal processing, and deep learning. She served as a reviewer for several journals such as IEEE Communication Magazine. She also served as a Technical Program Committee (TPC) Member for several conference.



Yuanhao Cui (Member, IEEE) received the B.Eng. degree (Hons.) from Henan University and the Ph.D. degree from the Beijing University of Posts and Telecommunications (BUPT). He has been the CTO and the Co-Founder of two startup companies, where he has invested more than \$3 million dollars. He holds more than 20 granted patents. His research interests include precoding and protocol designs for ISAC. He is a member of the IMT-2030 (6G) ISAC Task Group. He received the Best Paper Award from IWCMC 2021. He is the Founding Secretary of the IEEE ComSoc ISAC Emerging Technology Initiative (ISAC-ETI) and the CCF Science Communication Working Committee. He was the Organizer and the Co-Chair for a number of workshops and special sessions in flagship IEEE conferences, including ICC, ICASSP, WCNC, and VTC. He is the Lead Guest Editor for the Special Issue on Integrated Sensing and Communication for 6G of the IEEE OPEN JOURNAL OF THE COMMUNICATIONS SOCIETY and the Guest Editor for the Special Issue on Integrated Sensing and Communications for Future Green Networks of the IEEE TRANSACTIONS ON GREEN COMMUNICATIONS AND NETWORKING.



Zhaohui Yang (Member, IEEE) received the Ph.D. degree from Southeast University, Nanjing, China, in 2018. From 2018 to 2020, he was a Postdoctoral Research Associate with the Center for Telecommunications Research, Department of Informatics, King's College London, London, U.K. From 2020 to 2022, he was a Research Fellow with the Department of Electronic and Electrical Engineering, University College London, London. He is currently a ZJU Young Professor with the Zhejiang Key Laboratory of Information Processing Communication and Net-

working, College of Information Science and Electronic Engineering, Zhejiang University, Hangzhou, China, and also a Research Scientist with the Zhejiang Laboratory. His research interests include joint communication, sensing, computation, federated learning, and semantic communication. He was the recipient of the 2023 IEEE Marconi Prize Paper Award, 2023 IEEE Katherine Johnson Young Author Paper Award, 2023 IEEE ICCCN Best Paper Award, and the first Prize in Invention and Entrepreneurship Award of the China Association of Inventions. He was the Co-Chair of international workshops with more than ten times, including IEEE ICC, IEEE GLOBECOM, IEEE WCNC, IEEE PIMRC, and IEEE INFOCOM. He is an Associate Editor for the IEEE COMMUNICATIONS LETTERS, IET Communications, and EURASIP Journal on Wireless Communications and Networking. He was the Guest Editor for several journals, including IEEE JOURNAL ON SELECTED AREAS IN COMMUNICATIONS.



Weijie Yuan (Member, IEEE) received the B.E. degree from the Beijing Institute of Technology, Beijing, China, in 2013, and the Ph.D. degree from the University of Technology Sydney, Sydney, NSW, Australia, in 2019. From 2019 to 2021, he was a Research Associate with the University of New South Wales, Sydney, NSW, Australia. He is currently an Assistant Professor with the School of System Design and Intelligent Manufacturing, Shenzhen, China. He was a Research Assistant with the University of Sydney, Sydney, NSW, Australia,

a Visiting Associate Fellow with the University of Wollongong, Wollongong, NSW, Australia, and a Visiting Fellow with the University of Southampton, Southampton, U.K., from 2017 to 2019. In 2016, he was a Visiting Ph.D. Student with the Institute of Telecommunications, Vienna University of Technology, Austria. His research interests include statistical signal processing, OTFS, and ISAC. He is the CoChair and Co-Organizer for workshops and special sessions on orthogonal time frequency space (OTFS), and integrated sensing and communication (ISAC) in ICC 2021, ICC 2021, SPAWC 2021, VTC 2021-Fall, WCNC 2022, and ICASSP 2022. He is the Founding Chair of the IEEE ComSoc special interest group on OTFS (OTFS-SIG) and is serving as an Associate Editor for the EURASIP Journal on Advances in Signal Processing.



Xiaojun Jing (Member, IEEE) received the M.S. and Ph.D. degrees from the National University of Defense Technology in 1995 and 1999, respectively. He is currently a Professor at the Beijing University of Posts and Telecommunications. His research interests include wireless communication, information security, and image processing.